ACS APPLIED MATERIALS & INTERFACES

Research Article

www.acsami.org

Study of Nitrogen High-Pressure Annealing on InGaZnO Thin-Film Transistors

Seokhyun Yoon,[†] Young Jun Tak,[†] Doo Hyun Yoon,[†] Uy Hyun Choi,[†] Jin-Seong Park,[‡] Byung Du Ahn,*[,†] and Hyun Jae Kim*[,†]

[†]School of Electrical and Electronic Engineering, Yonsei University, 50 Yonsei-ro, Seodaemun-gu, Seoul, 120-749, Republic of Korea

[‡]Division of Materials Science and Engineering, Hanyang University, 222 Wangsimni-ro, Seoul 133-719, Republic of Korea

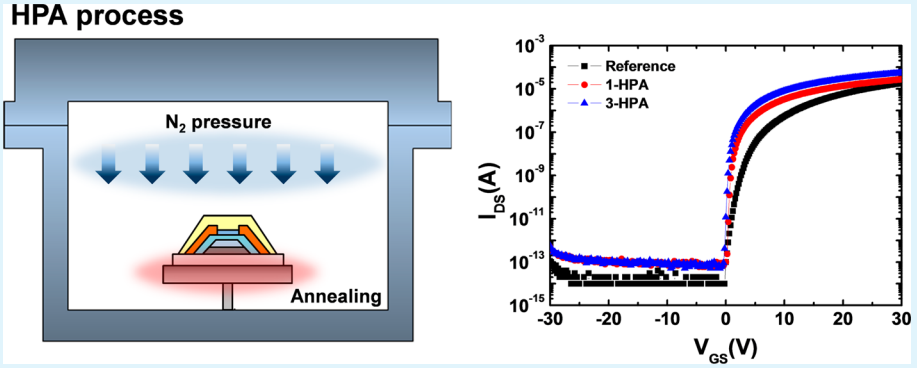

ABSTRACT: We studied the effects of high-pressure annealing (HPA) on InGaZnO (IGZO) thin-film transistors (TFTs). HPA was proceeded after TFT fabrication as a post process to improve electrical performance and stability. We used N_2 as the pressurized gas. The applied pressures were 1 and 3 MPa at 200 °C. For N_2 HPA under 3 MPa at 200 °C, field-effect mobility and the threshold voltage shift under a positive bias temperature stress were improved by 3.31 to 8.82 $cm^2/(V\ s)$ and 8.90 to 4.50 V, respectively. The improved electrical performance and stability were due to structural relaxation by HPA, which leads to increased carrier concentration and decreased oxygen vacancy.

KEYWORDS: *high-pressure annealing, InGaZnO, post process, thin-film transistor, oxide thin-film transistor*

1. INTRODUCTION

Oxide thin-film transistors (TFTs) have many strengths, such as a high mobility, high transparency, low off current, high uniformity, and a variety of deposition methods by simple processes.[1−6] As a result, oxide TFTs have been intensively researched to challenge amorphous Si-based TFTs in the display industry and for adoption in backplanes for the next-generation flat panel display industry. The application fields of oxide TFTs include liquid crystal,[7] 3D,[8] high resolution,[9] flexible,[10] and organic light-emitting diode displays.[8−10] Higher mobility and flexibility make oxide TFTs advantageous relative to Si-based TFTs. Many companies have already produced display products using oxide TFTs. However, to become the mainstream for backplanes in the display industry, some issues must be solved. These include lower stability, not enough mobility for above ultrahigh definition display, and an immature manufacturing process. Much research has been performed to overcome the above issues, including studies of channel materials and composition,[11−13] investigations of structures,[14−16] and applications of additional treatments.[17−19]

Recently, high-pressure annealing (HPA) has been researched for improved electrical characteristics and stability.[19−21] Among approaches used to overcome the drawbacks of oxide TFTs such as their mobility and stability, HPA has been studied for both solution and vacuum processes. In solution process, HPA was an in situ process for thin-film formation. Therefore, high-performance devices at low temperature could be fabricated, because pores in thin films were decreased by densification.[20] In vacuum process, HPA was conducted as a post treatment to reduce oxygen-related defects.[19,21] Therefore, the positive bias temperature stress (PBTS)[19] and negative bias temperature illumination stress (NBTIS)[21] results of InGaZnO (IGZO) TFTs were enhanced by decreasing oxygen vacancies in deep levels. In previous research, HPA was used with pressurized gases such as oxygen[20] and H_2O.[19,21] However, these gases could affect the electrical characteristics of oxide TFTs without HPA. Therefore, it is hard to know if the improved electrical performance by HPA can be attributed to HPA or pressurized gas effects. However, there has been no research on the effects of HPA on oxide semiconductors, despite its importance. Here, we focus the HPA effects themselves using N_2 as the pressurized gas, which was treated as inert gas.

Received: April 28, 2014
Accepted: July 31, 2014
Published: July 31, 2014

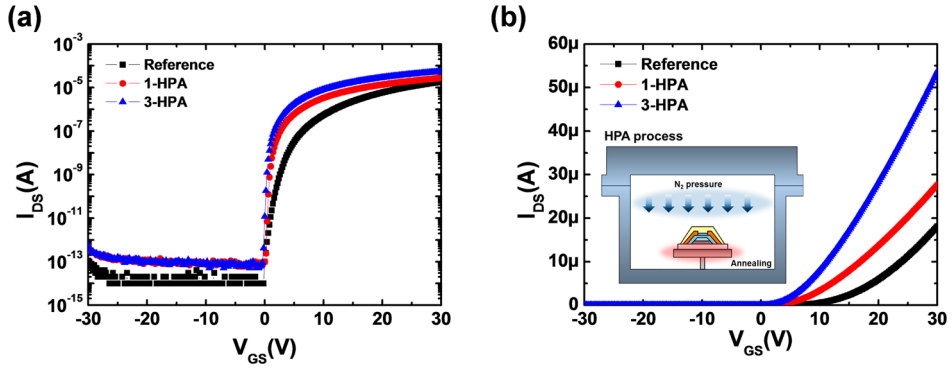

Figure 1. Transfer curves of the reference, 1-HPA, and 3-HPA with (a) log and (b) linear scales for I_{DS} (inset image is the schematic of HPA process).

Table 1. Electrical Properties of the Reference, 1-HPA, and 3-HPA

condition	μ_{FET} (cm^2/(V s))	on/off ratio	S.S (V/dec.)	N_{max} (/cm^2)	V_{TH} (V)	N_{ind} (/cm^2)
reference	3.31	1.81×10^9	0.48	6.78×10^{11}	7.16	
1-MPa	4.24	4.62×10^9	0.36	4.80×10^{11}	1.42	5.52×10^{11}
3-MPa	8.82	1.07×10^9	0.33	4.37×10^{11}	0.67	6.23×10^{11}

2. EXPERIMENTAL METHODS

2.1. Fabrication of IGZO TFTs. IGZO TFTs were prepared with an inverted staggered structure with an etch stopper layer (ESL). A MoW gate electrode was used and deposited by a sputtering system. The gate insulator, ESL, and passivation layer were SiO_2 using plasma-enhanced chemical vapor deposition. The IGZO channel layer was deposited by a sputtering system (IGZO target; In_2O_3:Ga_2O_3:ZnO = 2:2:1 mol %) and patterned with a width of 14 μm and length of 10 μm. Mo was used as the source/drain electrode, and deposited by sputtering system. After the TFTs were fabricated, they were postannealed at 300 °C for 1 h in ambient. HPA was conducted at 200 °C for 2 h in a N_2 atmosphere after finished TFT fabrication (inset image of Figure 1a). The pressurized pressures were 1 and 3 MPa. There were three experimental samples used to study the high-pressure effect: nonannealed (reference), annealed at 200 °C for 2 h under a 1 MPa N_2 atmosphere (1-HPA), and annealed at 200 °C for 2 h under a 3 MPa N_2 atmosphere (3-HPA).

2.2. Characterization of IGZO TFTs. Electrical characteristics of IGZO TFTs were measured with an HP 4156C semiconductor parameter analyzer in ambient. Transfer characteristics were measured under V_{DS} = 10.1 V and V_{GS} from −30 to 30 V. To analyze the positive bias stability, a PBTS test was performed under V_{GS} = 20 V and V_{DS} = 0.1 V at 60 °C for 15 000 s. To investigate IGZO thin films as a function of pressure, we used spectroscopic ellipsometry (SE) and X-ray photoelectron spectroscopy (XPS).

3. RESULTS AND DISCUSSION

Figure 1 shows the transfer characteristics of three samples, the reference, 1-HPA, and 3-HPA, with log (Figure 1a) and linear (Figure 1b) scales for I_{DS}. Electrical parameters, such as the field-effect mobility (μ_{FET}), on/off ratio, subthreshold swing (S.S), equivalent maximum density of states between channel and gate insulator (N_{max}), threshold voltage (V_{TH}), and the induced carrier concentration (N_{ind}), which was net-created carrier by HPA were summarized in Table 1. N_{max} was calculated using the following equation[22]

$$N_{max} = \left(\frac{\text{S. Slog}(e)}{kT/q} - 1 \right) \frac{C_i}{q} \quad (1)$$

where k is the Boltzmann constant, T is absolute temperature, q is the electron charge, and C_i is the capacitance of the gate insulator. N_{ind} was calculated as

$$N_{ind} = \frac{C_i \Delta V_{TH}}{q} \quad (2)$$

where ΔV_{TH} is the V_{TH} shift by post process, in this case HPA. μ_{FET} was 3.31 cm^2/(V s) for the reference, 4.24 cm^2/(V s) for 1-HPA, and 8.82 cm^2/(V s) for 3-HPA. It was therefore improved by 28% for 1-HPA and 166% for 3-HPA. Moreover, as shown in Figure 2, ΔV_{TH} under PBTS was also decreased as the applied pressure was increased. ΔV_{TH} under PBTS at 15000 s were 8.90, 4.95, and 4.50 V for the reference, 1-HPA, and 3-HPA, respectively. In other words, PBTS results were improved by 44% for 1-HPA and 49% for 3-HPA. From these results, we determined that HPA was an effective treatment for improving electrical parameters and stability. These enhancements were caused by modulating defect states near the conduction band minimum (CBM) and decreasing the oxygen vacancy.

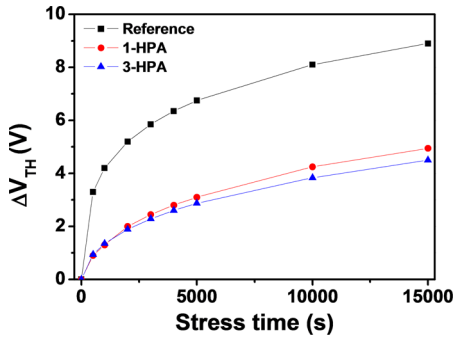

Figure 2. ΔV_{TH} under PBTS for the reference, 1-HPA, and 3-HPA.

Figure 3c shows the band alignments of three samples using SE and XPS. Figure 3a shows that the band offsets between the Fermi level (E_F) and the valence band maximum ($E_{FV} = E_V - E_C$), and the band offsets between the Fermi level (E_F) and CBM ($E_{CF} = E_C - E_F$) can be calculated using E_{FV}. The bandgaps (E_g) increased with the N_2 pressure, as shown in Figure 3b. In semiconductor physics, the electron concentration (n) can be calculated as

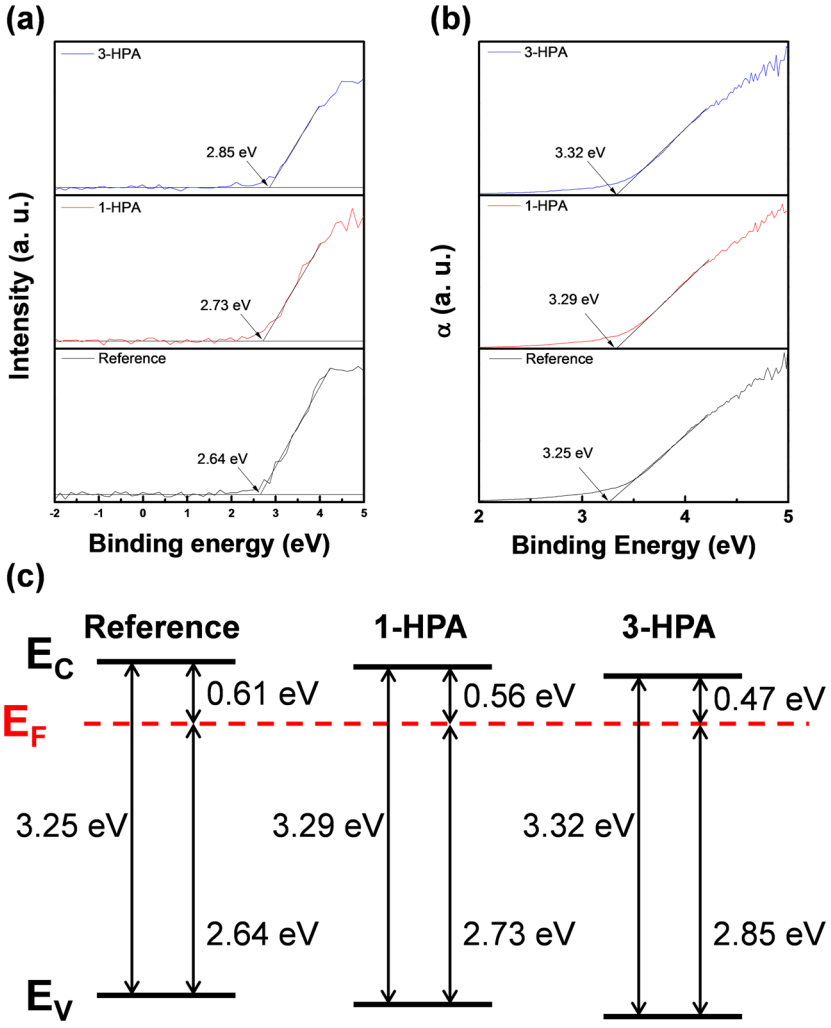

Figure 3. (a) XPS spectra near the valence band. (b) SE spectra of the absorption coefficient. (c) Band alignment of the reference, 1-HPA, and 3-HPA using XPS and SE data.

$$n = N_C \exp\left[-\frac{E_{CF}}{kT}\right] \quad (3)$$

where N_c is the effective density of states at the conduction band edge. Equation 3 shows that the electron concentration increases as E_{CF} was decreases. In the percolation model, the higher the carrier concentration, the higher Hall mobility appeared in oxide semiconductors.[23]

As shown in Figure 3c, E_{CF} decreased as the applied N_2 pressure increased. The decreased E_{CF} can explain the increased Hall mobility under N_2 HPA because a decreased E_{CF} leads to increased carrier concentration. In addition, E_g was increased by HPA. In general, E_g can be varied by increased carrier concentration through the combination of two opposite effects: bandgap widening from the Burstein−Moss effect,[23−25] and bandgap narrowing from a many-body interaction between free carriers or free carriers and ionized impurities.[26,27] E_g usually increases with the carrier concentration in oxide semiconductors, because the bandgap widening effect is dominant.[26,27] For IGZO thin films in particular, E_g and the carrier concentration are increased by structural relaxation,[28] which reduces the localized state near the CBM. This experiment showed similar results to the literature[26−28] in terms of E_g and the carrier concentration variation. As shown in eq 2, a negative shift of V_{TH} under post process creates an additional charge, which is N_{ind}. N_{ind} was 5.52 × 10^{11} /cm^2 for 1-HPA and 6.23 × 10^{11} /cm^2 for 3-HPA. Generally, for oxide TFTs, μ_{FET} was increased with Hall mobility.[29−32] Therefore, increased carrier concentration leads to higher electrical performance.

Figure 4 shows an analysis of the subgap state of the channel layer using SE analysis. Figure 4a shows two deconvoluted defect states (D1 and D2) with the Gaussian model form SE peaks near the conduction band. Figure 4b shows the relative areas of D1 and D2, and Figure 4c shows the peak position of D1 and D2 away from the CBM. The relative area of D1 was increased, and that of D2 was decreased as the applied pressure was increased. Figure 4d shows renewed band alignment with D1 and D2 using XPS (E_{FV}) and SE (E_g, D1, and D2) data. In general, D1 represents a shallow-level defect, which implies a donor-like state, and D2 represents a deep-level defect, which implies an acceptor-like state. As shown in panels b and c in Figure 4, the D1 peak position was shifted to CBM, and the relative area of D1 was increased as the N_2 applied pressure increased. This means that more free electrons were generated by the increased relative area of D1, and the generated free electrons were easily moved to the CBM.[33] In other words, generated free electrons lead to increased mobility by HPA.[23] However, the relative area of D2 was decreased by HPA. That means that the number of electron trapping sites was decreased. Moreover, N_{max} was decreased by

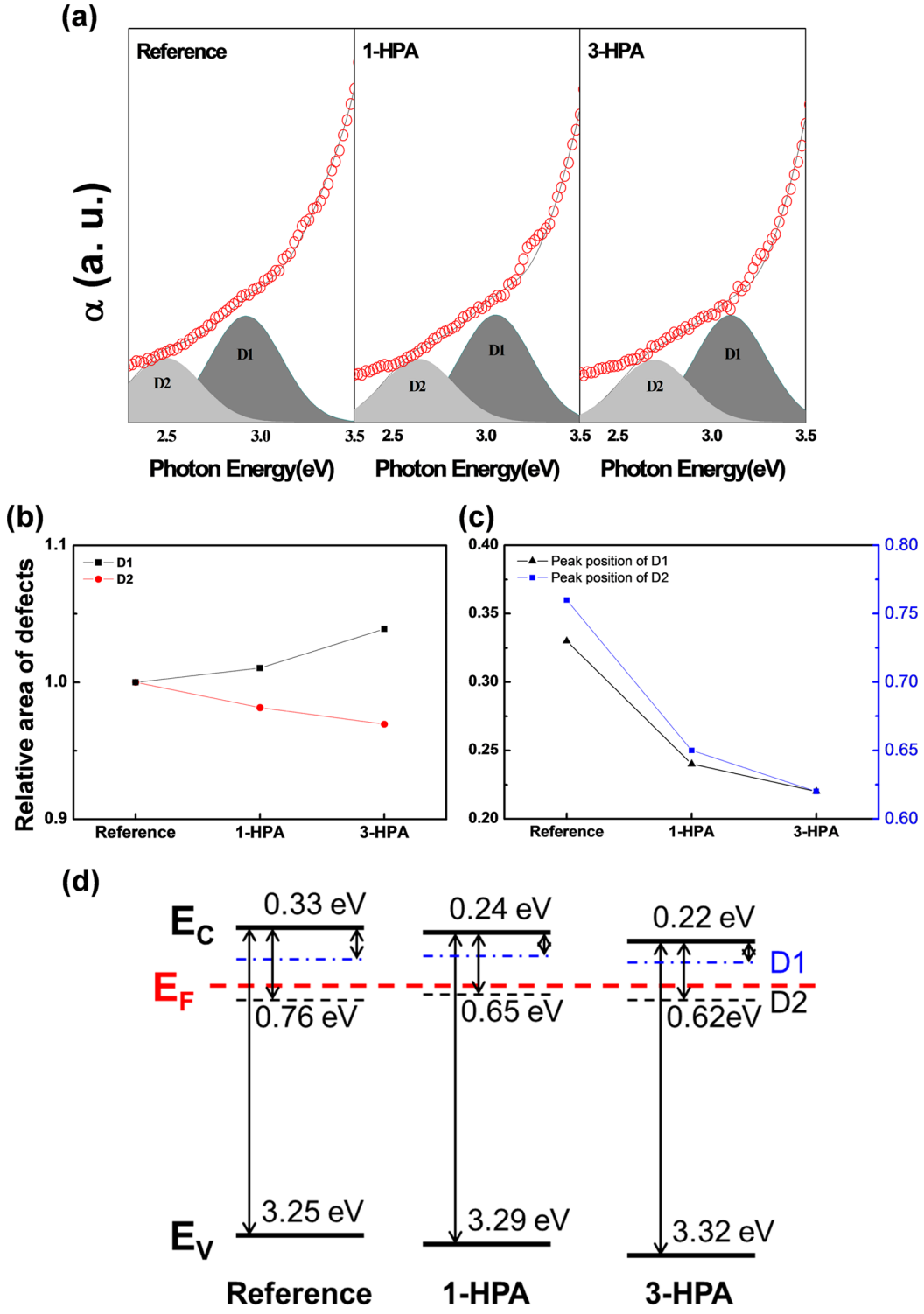

Figure 4. (a) SE spectra of absorption coefficients near the conduction band with deconvolution of two defect states (D1 and D2). (b) Relative area of the defects of the reference, 1-HPA, and 3-HPA. (c) Peak position of the defects of the reference, 1-HPA, and 3-HPA. (d) Band alignment of the reference, 1-HPA, and 3-HPA using XPS and SE data with D1 and D2 states.

29% for 1-HPA and 36% for 3-HPA. These were also plausible explanations for the increased mobility by HPA.

Figure 5a–c show O 1s peaks from XPS analysis for the reference, 1-HPA, and 3-HPA. XPS data were calibrated using the C 1s peak centered at 284.8 eV, and O 1s peaks were deconvoluted into three peaks, which were centered at 532, 531, and 530 ± 0.1 eV. The lower binding energy peak represented a metal oxide lattice without oxygen vacancy, the medium binding energy peak represented a metal oxide lattice with oxygen vacancy, and the higher biding peak represented metal hydroxide species. Figure 5d shows the relative area with oxygen vacancy in the metal oxide lattice (O_{vac}') and without oxygen vacancy in the metal oxide lattice (M-O′). Generally, the instability origin of positive bias stress originated from the electron trap sites which

dx.doi.org/10.1021/am502571w | ACS Appl. Mater. Interfaces 2014, 6, 13496–13501

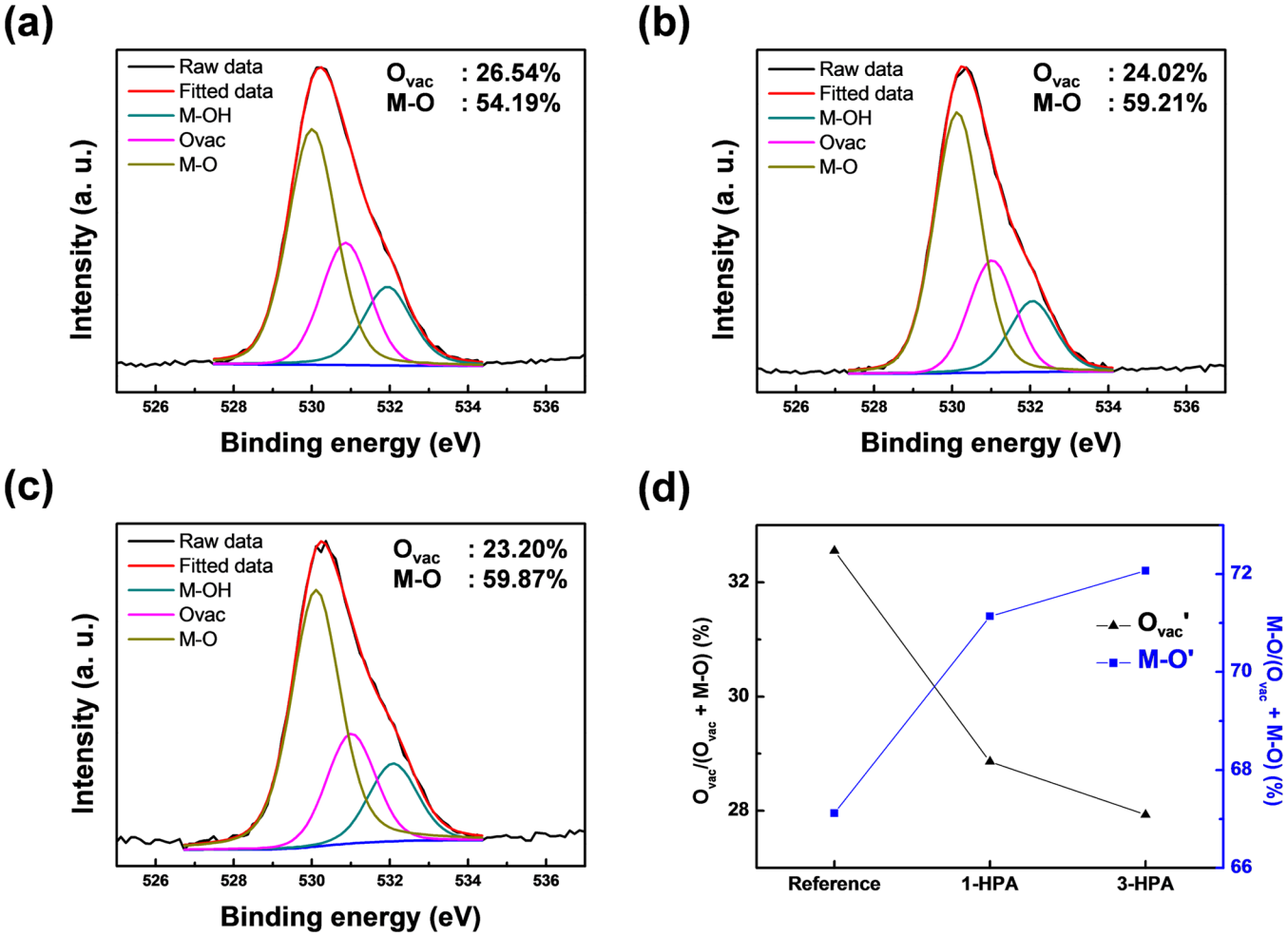

Figure 5. O 1s peaks from XPS analysis: (a) reference, (b) 1-HPA, and (c) 3-HPA. (d) O_{vac} in the metal oxide lattice (O_{vac}') and M-O in the metal oxide lattice (M-O′).

were oxygen vacancy in oxide semiconductors.[34,35] Compared to the reference, the relative area of the medium binding area (O_{vac}) was decreased 9% for 1-HPA and 13% for 3-HPA, whereas that of the lower binding area (M-O) was increased 9% for 1-HPA and 10% for 3-HPA. Moreover, O_{vac}' was also decreased from 32.88 to 27.93%. Therefore, HPA increased the film quality of IGZO thin films through increased M-O′ and decreased O_{vac}', and improved positive bias stability through decreased O_{vac}'

4. CONCLUSION

We investigated HPA-treated IGZO TFTs under a N_2 atmosphere. Structural relaxation occurred due to HPA, and carrier concentration and mobility were increased. As N_2 pressure was applied, the electrical properties and stability were improved due to increased shallow-level defects and decreased oxygen vacancies and deep-level defects. μ_{FET}, S.S, and ΔV_{TH} under PBTS improved 3.31 to 8.82 $cm^2/(V\,s)$, 0.48 to 0.33 V/dec., and 8.90 to 4.50 V, respectively. Therefore, we confirmed that HPA was a simple and effective method to improve electrical performance by structural relaxation.

AUTHOR INFORMATION

Corresponding Authors

*E-mail: hjk3@yonsei.ac.kr.
*E-mail: bdahn@yonsei.ac.kr.

Notes

The authors declare no competing financial interest.

ACKNOWLEDGMENTS

This work was supported by the National Research Foundation of Korea (NRF) grant funded by the Korean Ministry of Education, Science and Technology (MEST) (2011-0028819).

REFERENCES

(1) Nomura, K.; Ohta, H.; Ueda, K.; Kamiya, T.; Hirano, M.; Hosono, H. Thin-Film Transistor Fabricated in Single-Crystalline Transparent Oxide Semiconductor. *Science* **2003**, *300*, 1269−1272.
(2) Nomura, K.; Ohta, H.; Takagi, A.; Kamiya, T.; Hirano, M.; Hosono, H. Room-Temperature Fabrication of Transparent Flexible Thin-Film Transistors Using Amorphous Oxide Semiconductors. *Nature* **2004**, *432*, 488−492.
(3) Kamiya, T.; Hosono, H. Material Characteristics and Applications of Transparent Amorphous Oxide Semiconductors. *NPG Asia Mater.* **2010**, *2*, 15−22.
(4) Fortunato, E.; Barquinha, P.; Martins, R. Oxide Semiconductor Thin-Film Transistors: A Review of Recent Advances. *Adv. Mater.* **2012**, *24*, 2945−2986.
(5) Heo, S. J.; Yoon, D. H.; Jung, T. S.; Kim, H. J. Recent Advances in Low-Temperature Solution-Processed Oxide Backplanes. *J. Inf. Dispersion* **2013**, *14*, 79−87.
(6) Kim, S. J.; Yoon, S.; Kim, H. J. Review of Solution-Processed Oxide Thin-Film Transistors. *Jpn. J. Appl. Phys.* **2014**, *53*, 02BA02.

(7) Lee, J.-H.; Kim, D.-H.; Yang, D.-J.; Hong, S.-Y.; Yoon, K.-S.; Hong, P.-S.; Jeong, C.-O.; Park, H.-S.; Kim, S. Y.; Lim, S. K.; Kim, S. S.; Son, K.-S.; Kim, T.-S.; Kwon, J.-Y.; Lee, S.-Y. World's Largest (15-in.) XGA AMLCD Panel Using IGZO Oxide TFT. *Dig. Technol. Pap.—Soc. Inf. Dispersion Int. Symp.* **2008**, *39*, 625−628.
(8) Nam, W.-J.; Shim, J.-S.; Shin, H.-J.; Kim, J.-M.; Ha, W.-S.; Park, K.-H.; Kim, H.-G.; Kim, B.-S.; Oh, C.-H.; Ahn, B.-C.; Kim, B.-C.; Cha, S.-Y. 55-in. OLED TV using InGaZnO TFTs with WRGB Pixel Design. *Dig. Technol. Pap.—Soc. Inf. Dispersion Int. Symp.* **2013**, *44*, 243−246.
(9) Zhang, M.; Wang, G.; Lee, S.-K.; Lee, W.-B.; Liu, X.; Yuan, G.-C.; Xu, Y.-B.; Yoon, Y.-J.; Yang, H.-P.; Chen, J.; Park, H.-J.; Dong, Y.-M. Development of Large-Size Oxide TFT-LCD TV with ADSDS Technology. *Dig. Technol. Pap.—Soc. Inf. Dispersion Int. Symp.* **2013**, *44*, 104−106.
(10) Park, J.-S.; Kim, T.-W.; Stryakhilev, D.; Lee, J.-S.; An, S.-G.; Pyo, Y.-S.; Lee, D.-B.; Mo, Y. G.; Jin, D.-U.; Chung, H. K. Flexible Full Color Organic Light-Emitting Diode Display on Polyimide Plastic Substrate Driven by Amorphous Indium Gallium Zinc Oxide Thin-Film Transistors. *Appl. Phys. Lett.* **2009**, *95*, 013503.
(11) Barquinha, P.; Pereira, L.; Goncalves, G.; Martins, R.; Fortunato, E. Toward High-Performance Amorphous GIZO TFTs. *J. Electrochem. Soc.* **2009**, *156*, H161−H168.
(12) Iwasaki, T.; Itagaki, N.; Den, T.; Kumomi, H.; Nomura, K.; Kamiya, T.; Hosono, H. Combinatorial Approach to Thin-Film Transistors Using Multicomponent Semiconductor Channels: An Application to Amorphous Oxide Semiconductors in In−Ga−Zn−O System. *Appl. Phys. Lett.* **2007**, *90*, 242114.
(13) Kim, G. H.; Jeong, W. H.; Ahn, B. D.; Shin, H. S.; Kim, H. J.; Kim, H. J.; Ryu, M.-K.; Park, K.-B.; Seon, J.-B.; Lee, S.-Y. Investigation of the Effects of Mg Incorporation into InZnO for High-Performance and High-Stability Solution-Processed Thin-Film Transistors. *Appl. Phys. Lett.* **2010**, *96*, 163506.
(14) Kim, D. J.; Kim, D. L.; Rim, Y. S.; Kim, C. H.; Jeong, W. H.; Lim, H. S.; Kim, H. J. Improved Electrical Performance of an Oxide Thin-Film Transistor Having Multistacked Active Layers Using a Solution Process. *ACS Appl. Mater. Interfaces* **2012**, *4*, 4001−4005.
(15) Kim, D. J.; Rim, Y. S.; Kim, H. J. Enhanced Electrical Properties of Thin-Film Transistor with Self-Passivated Multistacked Active Layers. *ACS Appl. Mater. Interfaces* **2013**, *5*, 4190−4194.
(16) Kim, C. H.; Rim, Y. S.; Kim, H. J. Chemical Stability and Electrical Performance of Dual-Active-Layered Zinc−Tin−Oxide/Indium−Gallium−Zinc−Oxide Thin-Film Transistors Using a Solution Process. *ACS Appl. Mater. Interfaces* **2013**, *5*, 6108−6112.
(17) Han, S.-Y.; Herman, G. S.; Chang, C.-H. Low-Temperature, High-Performance, Solution-Processed Indium Oxide Thin-Film Transistors. *J. Am. Chem. Soc.* **2011**, *133*, 5166−5169.
(18) Park, J.-S.; Jeong, J. K.; Mo, Y.-G.; Kim, H. D.; Kim, S.-I. Improvements in the Device Characteristics of Amorphous Indium Gallium Zinc Oxide Thin-Film Transistors by Ar Plasma Treatment. *Appl. Phys. Lett.* **2007**, *90*, 262106.
(19) Shin, H. S.; Rim, Y. S.; Mo, Y.-G.; Choi, C. G.; Kim, H. J. Effects of High-Pressure H_2O-Annealing on Amorphous IGZO Thin-Film Transistors. *Phys. Status Solidi A* **2011**, *208*, 2231−2234.
(20) Rim, Y. S.; Jeong, W. H.; Kim, D. L.; Lim, H. S.; Kim, K. M.; Kim, H. J. Simultaneous Modification of Pyrolysis and Densification for Low-Temperature Solution-Processed Flexible Oxide Thin-Film Transistors. *J. Mater. Chem.* **2012**, *22*, 12491−12497.
(21) Rim, Y. S.; Jeong, W.; Ahn, B. D.; Kim, H. J. Defect Reduction in Photon-Accelerated Negative Bias Instability of InGaZnO Thin-Film Transistors by High-Pressure Water Vapor Annealing. *Appl. Phys. Lett.* **2013**, *102*, 143503.
(22) Kagan, C. R.; Andry, P. *Thin-film Transistors*; Marcel Dekker: New York, 2003; p 87.
(23) Takagi, A.; Nomura, K.; Ohta, H.; Yanagi, H.; Kamiya, T.; Hirano, M.; Hosono, H. Carrier Transport and Electronic Structure in Amorphous Oxide Semiconductor, a-$InGaZnO_4$. *Thin Solid Films* **2005**, *486*, 38−41.
(24) Thakur, A.; Kang, S.-J.; Baik, J. Y.; Yoo, H.; Lee, I.-J.; Lee, H.-K.; Jung, S.; Park, J.; Shin, H.-J. Effects of Working Pressure on Morphology, Structural, Electrical and Optical Properties of a-InGaZnO Thin Films. *Mater. Res. Bull.* **2012**, *47*, 2911−2914.
(25) Nomura, K.; Kamiya, T.; Yanagi, H.; Ikenaga, E.; Yang, K.; Kobayashi, K.; Hirano, M.; Hosono, H. Subgap States in Transparent Amorphous Oxide Semiconductor, In−Ga−Zn−O, Observed by Bulk Sensitive X-Ray Photoelectron Spectroscopy. *Appl. Phys. Lett.* **2008**, *92*, 202117.
(26) Lu, J. G.; Fujita, S.; Kawaharamura, T.; Nishinaka, H.; Kamada, Y. Carrier Concentration Induced Band-Gap Shift in Al-Doped $Zn_{1-x}Mg_xO$ Thin-Films. *Appl. Phys. Lett.* **2006**, *89*, 262107.
(27) Abdolahzadeh Ziabari, A.; Rozati, S. M. Carrier Transport and Bandgap Shift in N-Type Degenerate ZnO Thin-Films: The Effect of Band Edge Nonparabolicity. *Physica B* **2012**, *407*, 4512−4517.
(28) Ide, K.; Nomura, K.; Hiramatsu, H.; Kamiya, T.; Hosono, H. Structural Relaxation in Amorphous Oxide Semiconductor, a-In-Ga-Zn-O. *J. Appl. Phys.* **2012**, *111*, 073513.
(29) Suzuki, T. I.; Ohtomo, A.; Tsukazaki, A.; Sato, F.; Nishii, J.; Ohno, H.; Kawasaki, M. Hall and Field-Effect Mobilities of Electrons Accumulated at a Lattice-Matched ZnO/ScAlMgO4 Heterointerface. *Adv. Mater.* **2004**, *16*, 1887−1890.
(30) Kim, G. H.; Ahn, B. D.; Shin, H. S.; Jeong, W. H.; Kim, H. J.; Kim, H. J. Effect of Indium Composition Ratio on Solution-Processed Nanocrystalline InGaZnO Thin Film Transistors. *Appl. Phys. Lett.* **2009**, *94*, 233501.
(31) Kim, Y.-H.; Han, M. K.; Han, J.-I.; Park, S. K. Effect of Metallic Composition on Electrical Properties of Solution-Processed Indium-Gallium-Zinc-Oxide Thin-Film Transistors. *IEEE Trans. Electron Devices* **2010**, *57*, 1009−1014.
(32) Seo, S.-J.; Choi, C. G.; Hwang, Y.-H.; Bae, B.-S. High Performance Solution-Processed Amorphous Zinc Tin Oxide Thin Film Transistor. *J. Phys. D: Appl. Phys.* **2009**, *42*, 035106−1014.
(33) Park, H.-W.; Park, J.-S.; Lee, J. H.; Chung, K.-B. Thermal Evolution of Band Edge States in ZnO Film as a Function of Annealing Ambient Atmosphere. *Electrochem. Solid State Lett.* **2012**, *15*, H133−H135.
(34) Kamiya, T.; Nomura, K.; Hirano, M.; Hosono, H. Electronic Structure of Oxygen Deficient Amorphous Oxide Semiconductor a-$InGaZnO_{4-x}$: Optical Analyses and First-Principle Calculations. *Phys. Status Solidi C* **2008**, *5*, 3098−3100.
(35) Noh, H.-K.; Chang, K. J.; Rue, B.; Lee, W.-J. Electronic Structure of Oxygen-Vacancy Defects in Amorphous In-Ga-Zn-O Semiconductors. *Phys. Rev. B* **2011**, *84*, 115205.